JOURNAL OF SOLID STATE CHEMISTRY 1, 66–81 (1969)

Mixed Oxides of Titanium and Niobium: Intergrowth Structures and Defects

J. G. ALLPRESS

Commonwealth Scientific and Industrial Research Organization
Division of Tribophysics, University of Melbourne,
Melbourne, Australia

Received January 15, 1969

The binary oxides of titanium and niobium, $TiNb_2O_7$, $Ti_2Nb_{10}O_{29}$, $TiNb_{24}O_{62}$ and $TiNb_{52}O_{132}$, have been examined by electron diffraction and microscopy. The structure of $TiNb_{52}O_{132}$, an ordered intergrowth of $TiNb_{24}O_{62}$ and high temperature Nb_2O_5, is clarified. There are many planar defects in these compounds which can be described in terms of the random intergrowth, at the unit cell level, of very thin fragments of other closely related phases. Similar intergrowths are found in regions of the phase diagram previously referred to as "solid solutions," and a number of ordered sequences characteristic of new phases are described.

1. Introduction

Traditional techniques for the detection and identification of phases in binary and more complex oxide systems involve the use of X-ray powder diffraction techniques and, to some extent, optical microscopy. In many cases, large regions of solid solution have been reported. During recent years, a reappraisal of some of these systems using refined X-ray powder and single crystal diffraction methods, have provided clear evidence for the existence of numbers of discrete, but closely related phases in regions which were previously considered to be solid solutions. A notable example is the system WO_3–Nb_2O_5, where five discrete compounds have been isolated and characterized by crystal structure analyses (*1*, *2*); all these phases contain less than 50 mole percent WO_3 and lie in a so called "solid solution" region (*3*, *4*). One of these phases (*2*) is an ordered intergrowth of two neighboring structures, and a further three intergrowth structures, all containing less than 10 mole percent WO_3, have been identified recently by electron diffraction and microscopy (*5*).

The situation is similar, but not so clear, in the system TiO_2–Nb_2O_5. Roth and Coughanour (*6*) reported two binary oxides $TiO_2 \cdot Nb_2O_5$, and $TiO_2 \cdot 3Nb_2O_5$, but the composition of the latter was not established with certainty. Wadsley (*7*, *8*) determined the crystal structures of these phases (Fig. 1), and showed that the latter is in fact $Ti_2Nb_{10}O_{29}$, and exists in monoclinic and orthorhombic forms. Subsequently, a new phase richer in Nb_2O_5 was reported (*9*) and its crystal structure analysis (*10*) identified it as $TiNb_{24}O_{62}$. (Fig. 1d). Another phase, $(Ti,Nb)O_{2.483}$ isostructural with $NbO_{2.483}$ was described by Gruehn and Norin (*11*). Norin's proposed structure (Fig. 4e) is an ordered intergrowth of $TiNb_{24}O_{62}$ and the high temperature (H) form of Nb_2O_5 (*12*), and has the composition $TiNb_{52}O_{132}$, i.e. $(Ti,Nb)O_{2.491}$. Apart from the discrepancy in composition, the primitive symmetry of this structure is incompatible with the reported powder diffraction data (*11*), in which all the observed reflexions are consistent with a body-centered structure i.e. $h + k + l = 2n$.

The close relationship between all these structures is clear from the idealized drawings in Fig. 1. They all contain fragments of the simple rhenium trioxide structure, in the form of blocks of corner-shared metal–oxygen octahedra. The different stoichiometries and structures of the phases are a consequence of variations in the size of these blocks and the way they are joined together. There is no evidence from any of the X-ray investigations for ordering of the Ti and Nb atoms; the metal positions in the structures are occupied by one or other of these elements in a random manner.

There are a number of possibilities for intergrowth among these structures. Some evidence for additional phases, possibly of this type, was obtained by Wadsley (*8*), who attempted to prepare a phase of composition $TiNb_{14}O_{37}$, containing blocks of

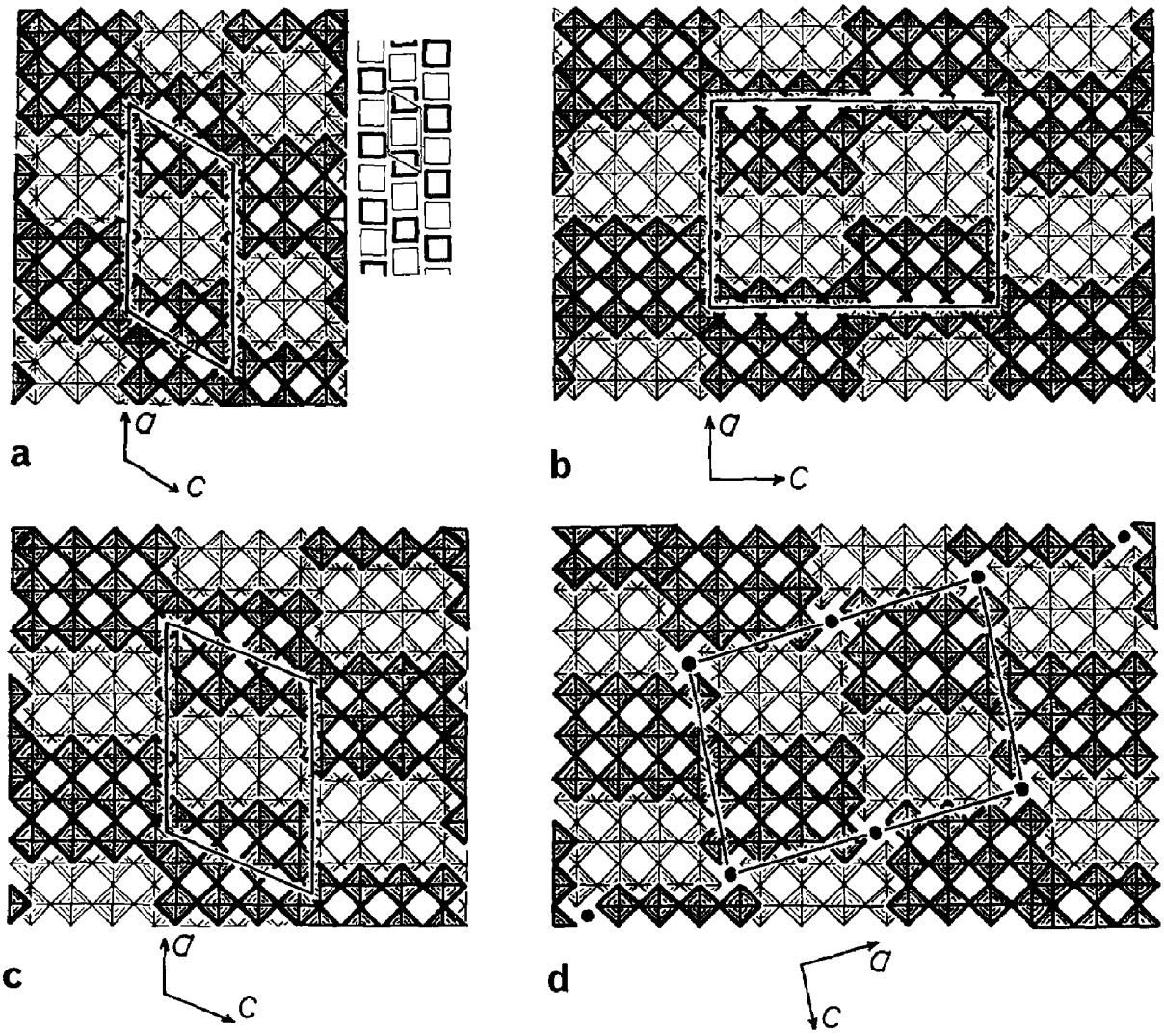

FIG. 1. Idealized models representing the structures of titanium niobium oxides. Each square represents an octahedron viewed down a body diagonal, the lighter and darker squares being centered on parallel planes 1.9 Å apart. The octahedra share corners within the structural blocks, and edges in the junctions, or shear planes, between the blocks. (a) $TiNb_2O_7$—the blocks are 3 octahedra × 3 octahedra in size. Right—simpler representation of this structure. Each block is represented by a square joining the corner metal atoms in the block (b) $Ti_2Nb_{10}O_{29}$ orthorhombic—3 × 4 blocks. (c) $Ti_2Nb_{10}O_{29}$ monoclinic—3 × 4 blocks. (d) $TiNb_{24}O_{62}$— 3 × 4 blocks. The circles represent metal atoms in tetrahedral coordination.

fifteen octahedra (3 wide × 5 long), but otherwise analogous to monoclinic $Ti_2Nb_{10}O_{29}$ (3 × 4 blocks) and $TiNb_2O_7$ (3 × 3 blocks). (The compound $MgNb_{14}O_{35}F_2$ (*13*) has since been found to have this structure). He did not obtain the desired phase, but noted that material of this composition "gave a bewildering variety of diffraction patterns, bearing considerable similarities to one another as well as to α—(i.e. H–)Nb_2O_5." Subsequently (*14*), he suggested that an intergrowth of $TiNb_2O_7$ and $Ti_2Nb_{10}O_{29}$ might exist, and attempted to prepare $Ti_5Nb_{16}O_{50}$, whose composition corresponds to a eutectic in the phase diagram. He found that when the component oxides were reacted at temperatures below the solidus, the product was a mixture of $TiNb_2O_7$ and $Ti_2Nb_{10}O_{29}$, but preparations quenched from the liquidus contained disordered sequences of fragments of the two phases.

Electron microscopy and diffraction have proved to be very useful in the study of defects and inter-

growth in the Nb_2O_5–WO_3 system (*5*, *15*). Electron diffraction patterns from small areas are quite sensitive to the presence of ordered structures, and transmission observations on suitably oriented thin crystals can reveal structural information at the unit cell level. This paper presents results obtained by the application of these techniques in the Nb_2O_5–TiO_2 system. In addition to the phases shown in Fig. 1, a number of samples of other compositions have been studied. The results and their interpretation are divided into sections, covering four ranges of composition i.e. Nb_2O_5–$TiNb_{24}O_{62}$, $TiNb_{24}O_{62}$–$Ti_2Nb_{10}O_{29}$, $Ti_2Nb_{10}O_{29}$–$TiNb_2O_7$, and $TiNb_2O_7$–TiO_2.

The defects described here are those which are caused by the presence of intergrowth; other more complex defects occur less frequently, and some of them will be discussed in a subsequent publication.

2. Experimental

2.1 Specimens

Most of the samples used in this study were provided by Dr. A. D. Wadsley of the Division of Mineral Chemistry, CSIRO, and were identical to those used for the earlier X-ray crystal structure investigations. Samples of $(Ti,Nb)O_{2.483}$ and $NbO_{2.483}$ were obtained from Dr. R. Gruehn of the University of Münster, Westphalia. Other mixed oxides of several different compositions (Nb_2O_5:TiO_2 = 40:1, 26:1, and 19:1) were also prepared for this present study. Because of the small amounts of TiO_2 in the mixtures, special care was taken to ensure homogeneous mixing of the two components. Two methods were used:

1. The mixtures were melted on platinum discs in an induction heater, and then annealed at temperatures up to 1400C in platinum boats in air.

2. The two metals were quantitatively co-precipated from solution and the precipitates were then ignited in air. The technique was based on that described by Milner, Barrett, and Smales (*16*). Standard solutions of Nb^{5+} (0.005 *M*) and Ti^{4+} (0.0005 *M*) were prepared by dissolving weighed amounts of the oxides in hot hydrofluoric acid solution, adding concentrated sulphuric acid, evaporating until fumes of sulphuric acid appeared, and diluting the solution to 500 ml with ammonium oxalate solution. Appropriate amounts of these solutions were mixed, neutralized with concentrated ammonia solution, and buffered with a 1 *M* ammonium acetate/acetic acid solution. The metals were then co-precipitated as the tannate complexes by adding solid tannic acid (>5 times the weight of metal to be precipitated) to the boiling solution. The flocculent red precipitate was filtered on sintered glass, washed with water, dried at 100C, ignited in a platinum crucible at 800C to decompose the

TABLE I

CRYSTALLOGRAPHIC DATA FOR Ti-Nb OXIDES

Compound	Mole percent Nb_2O_5	Unit cell dimensions Å				Z	Symmetry[a]	Ref.
		a	b	c	β			
$TiNb_2O_7$	50	20.44	3.81	11.93	120.2°	6	C	7
$Ti_2Nb_{10}O_{29}$	71.5	20.54	3.814	15.57	113.7°	2	C	8
$Ti_2Nb_{10}O_{29}$ (O)	71.5	20.51	3.805	28.50		4	O	8
$Ti_5Nb_{44}O_{120}$	81.5	29.7	3.82	41.1	100.3°	2	C	[b]
$Ti_3Nb_{34}O_{91}$	85.0	29.7	3.82	32.3	108.8°	2	C	[b]
$TiNb_{24}O_{62}$	92.3	29.78	3.821	21.21	94.9°	2	C	10
		29.7	3.82	20.9	94.7°			[b]
$TiNb_{38}O_{97}$	95.0	47.0	3.82	20.9	98.8°	2	P	[b]
		47.5	3.82	21.2	98.5°			[c]
$TiNb_{52}O_{132}$	96.3	65.6	3.82	21.2	104.5°	2	C	[c]
		65.6	3.82	20.9	104.9°			[b]

[a] C—side-centered monoclinic; P—primitive monoclinic (P2); O—side centered orthorhombic (Cmcm).
[b] This work—cell dimensions calculated from idealized models.
[c] This work—cell dimensions derived from electron diffraction data.

tannates, and finally heated in platinum boats at temperatures up to 1400C.

2.2 Electron Microscope Examination

The techniques for mounting the powdered specimens on grids and their subsequent examination in the electron microscope (Philips EM200) were the same as described previously (*15*).

3. Results and Interpretation

The unit cell dimensions and space group data, derived from previous X-ray studies for the compounds examined in this work, are collected in Table I. In all cases, the *b* axis is around 3.8 Å, the length of the octahedral body diagonal of the structures. The electron microscope observations have generally been made on thin crystals (or thin edges of crystals) which have been tilted until their *b* axes are approximately parallel to the incident electron beam. The diffraction patterns, with the exception of several from $TiNb_{52}O_{132}$ taken to check the space group extinctions (Fig. 2c,e) are all *h*0*l* sections of the reciprocal lattice. The areas of the crystals selected for diffraction were usually of the order of $1\mu^2$ (10^{-8} cm^2) and areas imaged by transmission were often considerably smaller than this.

In addition to the idealized models shown in Fig. 1, an even simpler representation of the structures (e.g. Fig. 1a, right) is useful. Each block of corner-shared octahedra is represented in projection by a rectangle outlining the corner metal atoms in the block. The interpretation of defect structures is greatly facilitated by the fact that the dimensions of compounds of this kind can be reliably estimated from the idealized models, assuming only that the edge-length of each octahedron is 2.89 Å (*15*).

For convenience, all the micrographs, the *h*0*l* diffraction patterns, and the structural drawings in this paper have been oriented consistently in such a way that lines of metal atoms in the blocks of octahedra run parallel to the edges of the page, and the blocks are always three octahedra in length in the direction up and down the page, e.g. parallel to *a* in Fig. 1a–c.

3.1 The Region Nb_2O_5–$TiNb_{24}O_{62}$.

3.1.1 *Electron Diffraction.* The *h*0*l* patterns of H–Nb_2O_5 and $TiNb_{24}O_{62}$ are shown in Fig. 2a,b. The similarity between them is striking, and it is not surprising that $TiNb_{24}O_{62}$ was not identified in the original phase analysis (*6*). Patterns from samples with compositions within this range (0–8 mole percent TiO_2) were also very similar and commonly showed a multiplicity of spots and streaks (e.g. Fig. 2d,f) along the reciprocal lattice rows in the direction corresponding to c^* in H–Nb_2O_5, and a^* in $TiNb_{24}O_{62}$. None of these samples was a single phase—the diffraction patterns of individual crystals within a sample often varied slightly from one to another. However, the composition $TiO_2 \cdot 26Nb_2O_5$ gave the most consistent patterns (Fig. 2c–e) and similar patterns were also frequently encountered in Gruehn's specimens of $NbO_{2.483}$ and $(Ti,Nb)O_{2.483}$. The X-ray powder diffraction patterns from $TiO_2 \cdot 26Nb_2O_5$, recorded on a Guinier focussing camera, also corresponded closely with the data reported by Norin for $NbO_{2.483}$ (*11*).

3.1.2 *Electron Microscopy.* The structural differences in this composition region are indicated in the diffraction patterns by changes along the reciprocal lattice rows parallel to the axis marked a^* in Fig. 2b,d,f. Hence transmission micrographs of crystals tilted to reveal the *h*00 set of reflections should be informative. (For H–Nb_2O_5, the corresponding reflections are 00*l*). Lattice image micrographs using these reflections are shown in Fig. 3 for H–Nb_2O_5, $TiNb_{24}O_{62}$ and samples of several intermediate compositions. Two different fringe spacings can be distinguished in these micrographs; (a) 17 Å fringes, characteristic of pure H–Nb_2O_5 and (b) 15 Å fringes, characteristic of pure $TiNb_{24}O_{62}$. In $TiO_2 \cdot 26Nb_2O_5$ (Fig. 3c) and also $(Ti,Nb)O_{2.483}$ (Fig. 3d) there are ordered sequences of these wide and narrow fringes. Measurements from microdensitometer records taken across similar micrographs show that the spacings are the same as those quoted above, within experimental error (ca. ±5%). Many samples contained areas where the sequence was ordered, as in the Regions X and Z in Fig. 3d, but in some cases the sequence appeared to be almost completely random (Fig. 3b, Region Y in Fig. 3d).

3.1.3 *The Structure of* $TiNb_{52}O_{132}$. The diffraction patterns and lattice image observations of $TiO_2 \cdot 26Nb_2O_5$ established that this was the same phase as the one described by Gruehn and Norin (*11*), and that its structure is an ordered intergrowth of H–Nb_2O_5 and $TiNb_{24}O_{62}$. However, it is clear from the single crystal electron diffraction data (Fig. 2c–e), that the unit cell is centered rather than primitive. The longest axis in the *h*0*l* section (Fig. 2d) is 32.8 Å, slightly more than half the value quoted by Norin (63.52 Å). The *hk*0 section (Fig. 2c) indicates that only those reflections for which $h + k = 2n$ are allowed. The dimensions of the side centered unit cell are given in Table I. The *a* axis corresponds to a diagonal of the unit cell reported by Norin for

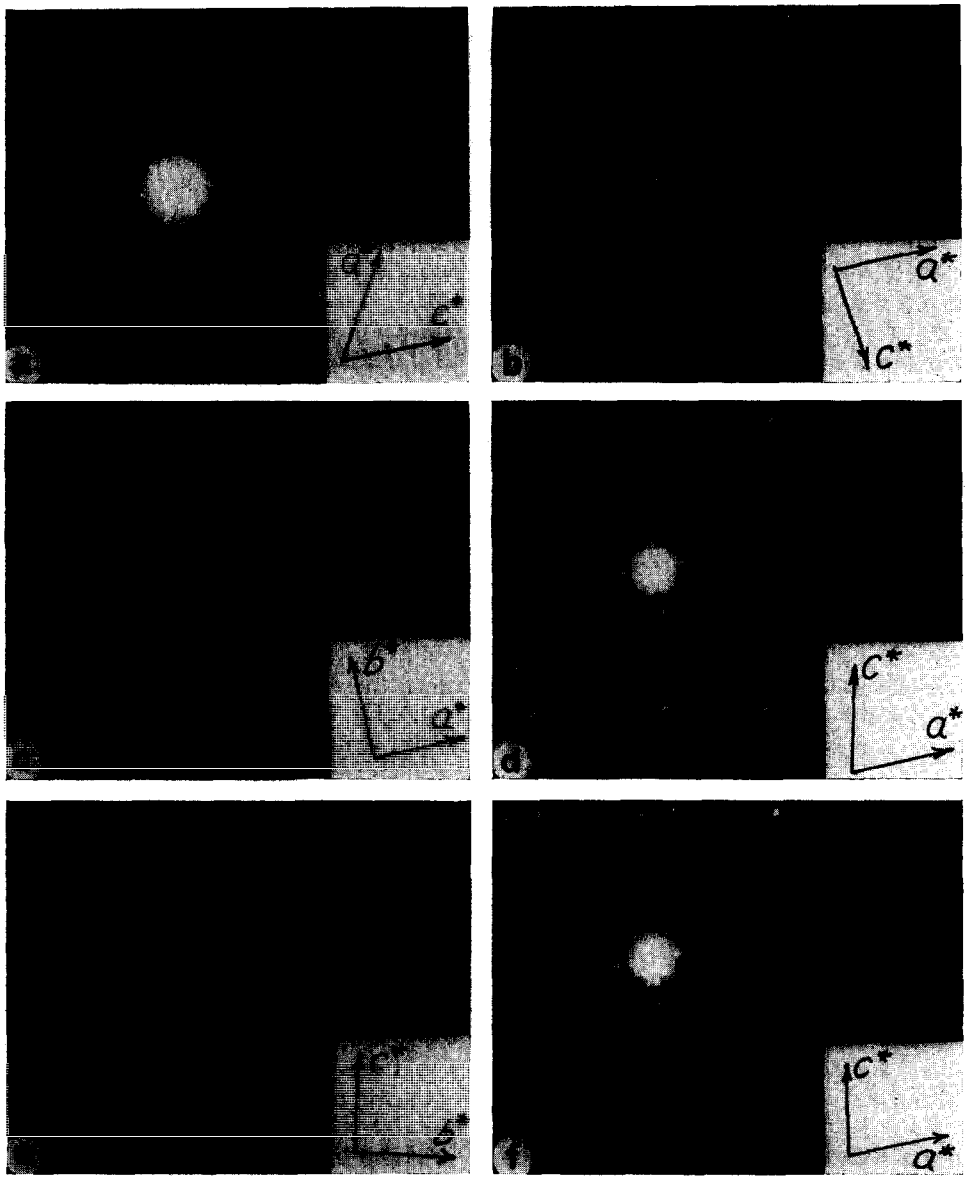

FIG. 2. Electron diffraction patterns of phases found in the region Nb_2O_5–$TiNb_{24}O_{62}$. (a) H–Nb_2O_5—*h0l* section; (b) $TiNb_{24}O_{62}$—*h0l* section; (c) $TiNb_{52}O_{132}$—*hk*0 section; (d) $TiNb_{52}O_{132}$—*h0l* section; (e) $TiNb_{52}O_{132}$—0*kl* section; (f) $TiNb_{38}O_{97}$—*h0l* section.

$NbO_{2.483}$ (Fig. 4e). When this alternative unit cell is chosen, Norin's data (*11*) becomes $a = 65.50$ Å, $b = 3.827$ Å, $c = 21.15$ Å, $\beta = 104.7°$ in good agreement with the dimensions obtained here for $TiO_2 \cdot 26Nb_2O_5$.

The 21 Å axis of the new phase is also found in $TiNb_{24}O_{62}$ and H–Nb_2O_5. In the direction of this axis, the two latter compounds contain rows of blocks of two types:

(i) In $TiNb_{24}O_{62}$ (Fig. 1d, 4a) the rows, referred to as C Rows (Fig. 4b) contain blocks which are four octahedra long by three wide. In any one row, these blocks lie alternately at two levels in the structure, centered 1.9 Å (= $b/2$) apart, and they are joined by sharing octahedral edges.

(ii) In H–Nb_2O_5 (Fig. 4c) the rows, referred to as D Rows (Fig. 4d) contain 4×3 blocks at one level, joined by sharing edges to 5×3 blocks at the other level. These rows differ from the rows identified as A and B in a previous publication (*5*), which were

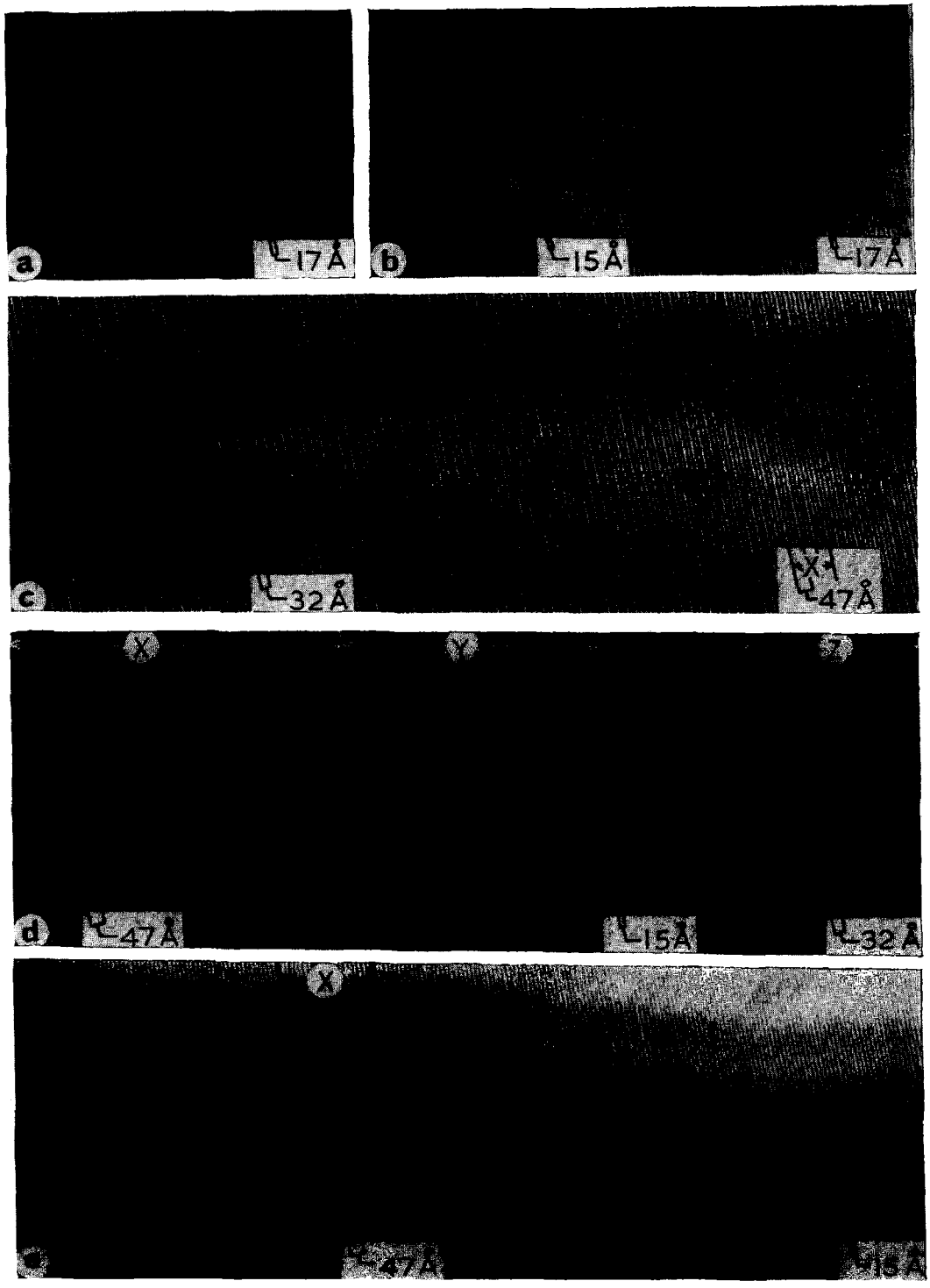

FIG. 3. Lattice images of crystals in samples with compositions in the region Nb_2O_5–$TiNb_{24}O_{62}$. Magnification: 450,000×. (a) H–Nb_2O_5; (b) $TiO_2 \cdot 40Nb_2O_5$; (c) $TiO_2 \cdot 26Nb_2O_5$—the Area X is a small domain of $TiNb_{38}O_{97}$; (d) $(Ti,Nb)O_{2.483}$—the Regions X, Y, and Z are predominantly $TiNb_{38}O_{97}$, $TiNb_{24}O_{62}$ and $TiNb_{52}O_{132}$, respectively. (e) $TiNb_{24}O_{62}$—the Area X is a domain of $TiNb_{38}O_{97}$.

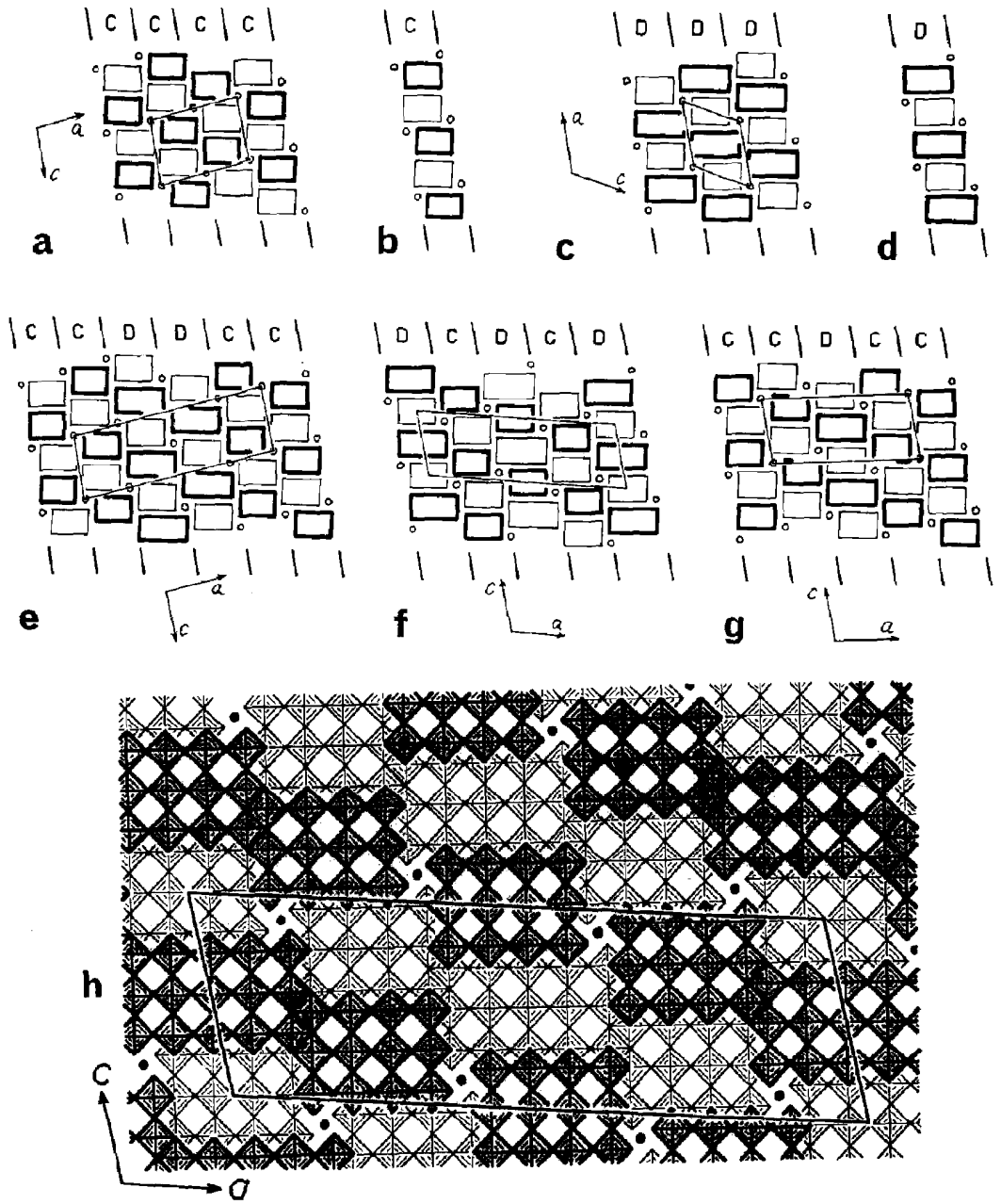

FIG. 4. Idealized models of the structures found in the region Nb_2O_5–$TiNb_{24}O_{62}$. The blocks of octahedra are represented by rectangles, the tetrahedral atoms by circles. The unit cell of each structure is outlined. The sets of parallel lines above and below each model indicate the position of shear planes in the structures. (a) $TiNb_{24}O_{62}$; (b) Component rows of $TiNb_{24}O_{62}$—C Rows; (c) H–Nb_2O_5; (d) Component rows of H–Nb_2O_5—D Rows; (e) $TiNb_{52}O_{132}$—structure proposed by Norin (*11*); (f) $TiNb_{52}O_{132}$—structure proposed in this paper; (g) $TiNb_{38}O_{97}$; (h) $TiNb_{52}O_{132}$, showing individual octahedra.

used to describe a series of intergrowths between H–Nb_2O_5 and $WNb_{12}O_{33}$. Thus the stacking of rows parallel to the 21 Å axis in $TiNb_{24}O_{62}$ is —C—C—C— and in H–Nb_2O_5 is —D—D—D—. Norin's proposed structure is an intergrowth of these two, with the stacking sequence

—C—C—D—D—C—C—D—D—

(Fig. 4e). A simpler sequence which gives the same composition is —C—D—C—D— and the corresponding model is shown in Fig. 4f. It has the same dimensions as Norin's structure, but possesses the correct symmetry. The unit cell (Fig. 4h) contains 106 metal-atom positions and 264 oxygen positions, the proposed composition is therefore $TiNb_{52}O_{132}$, with $Z = 2$.

The lattice images (Fig. 3c,d) provide direct confirmation of the stacking sequence

—C—D—C—D—C—

The regions in the structure where the rows are joined together, which may be referred to as crystallographic shear planes (*17*), are areas of higher-than-average atomic density, because the octahedra share edges rather than corners and the metal atoms are closer together than they are in the blocks. These shear planes might therefore be expected to appear in lattice images of thin crystals, which behave as phase gratings (*18*). In the proposed structure, the shear planes are not evenly spaced; the calculated separation is 16.8 Å across a D Row and 14.8 Å across a C Row. This is in reasonable agreement with the observed spacing of black fringes in the micrographs. If it existed, the —C—C—D—D— sequence in Norin's structure would give a distinctly different lattice image.

3.1.4 *Defects and Other Intergrowths.* Micrographs show that the intergrowth of C and D Rows need not be ordered, and many random sequences have been observed (e.g. Fig. 3b). It is a straightforward matter to make an idealized model for a particular sequence, and to show that these random intergrowth structures fit together coherently at the shear planes and there is therefore a negligible amount of strain for the accommodation of defects of this kind.

Other ordered sequences may occur; in particular the —D—C—C—D—C—C—D— sequence seen in the Region X in Fig. 3d,e is quite common. Domains of this sequence were often large enough to give discrete spots in diffraction patterns; the pattern from a particularly large region found in Gruehn's $(Ti,Nb)O_{2.483}$ is shown in Fig. 2f. A model of a structure with this sequence is shown in Fig. 4g. Its ideal composition is $TiNb_{38}O_{97}$, and its calculated unit cell dimensions agree well with those derived from the electron diffraction data (Table I).

The frequency with which domains of $TiNb_{38}O_{97}$ and also $TiNb_{24}O_{62}$ (Area Y in Fig. 3d) have been observed in Gruehn's samples of $(Ti,Nb)O_{2.483}$ suggests that the reason for the departure in composition of these samples from the ideal composition $TiNb_{52}O_{132}$ or $(Ti,Nb)O_{2.491}$, is due at least in part to the presence of domains of these other phases containing more titanium, and correspondingly less oxygen.

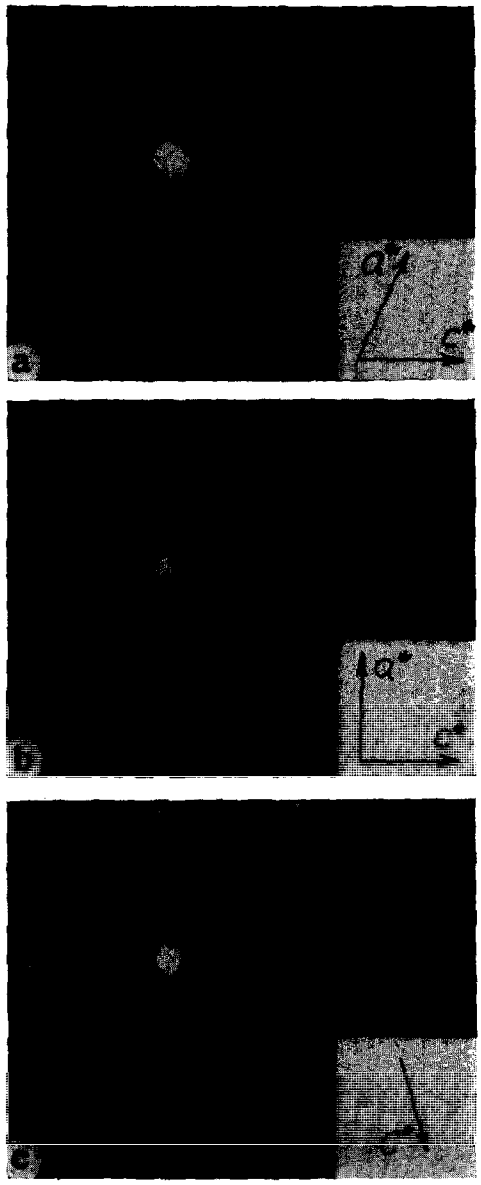

FIG. 5. Electron diffraction patterns (*h0l* reciprocal lattice sections) from: (a) monoclinic $Ti_2Nb_{10}O_{29}$; (b) orthorhombic $Ti_2Nb_{10}O_{29}$; (c) a crystal fragment in a sample of "$TiNb_{14}O_{37}$."

It seemed probable that homogeneous samples of

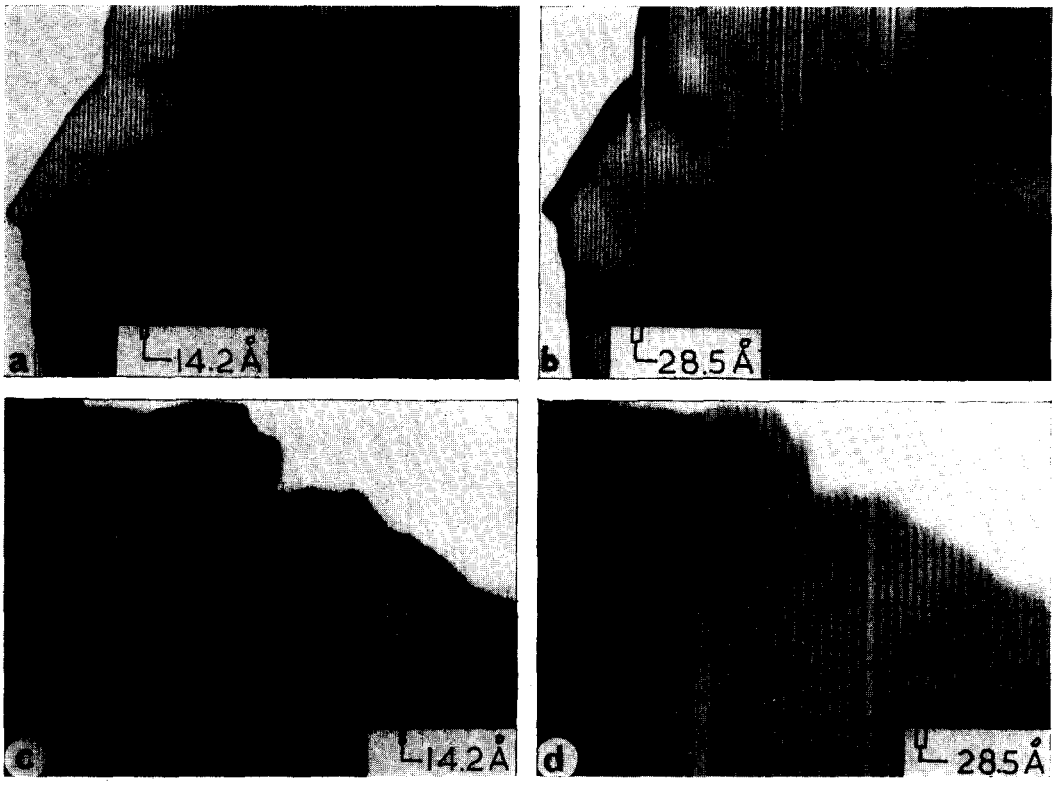

FIG. 6. Lattice images from crystals of $Ti_2Nb_{10}O_{29}$. Magnification 450,000×. (a) Monoclinic polymorph, imaged using 00*l* reflections. (b) Same crystal, tilted to reveal faulting. (c) Orthorhombic polymorph, imaged using 00*l* reflections. (d) Same crystal, tilted to reveal faulting.

$TiNb_{38}O_{97}$ and other, similar intergrowths such as $TiNb_{80}O_{202}$ (row sequence

—C—D—D—C—D—D—C—)

could be prepared. Mixtures of the compositions $TiO_2 \cdot 19Nb_2O_5$ and $TiO_2 \cdot 40Nb_2O_5$ were reacted and annealed at temperatures up to 1400C, but the conditions for the formation of large ordered regions of these intergrowths were not established.

3.2 The Region $TiNb_{24}O_{62}$–$Ti_2Nb_{10}O_{29}$.

3.2.1 *Electron Diffraction.* The *h*0*l* patterns for the monoclinic and orthorhombic forms (*8*) of $Ti_2Nb_{10}O_{29}$ are shown in Fig. 5a,b. The streaks which appear along the reciprocal lattice rows running parallel to c^* in the pattern of the monoclinic polymorph (Fig. 5a) are a common feature of this sample. The reason for this streaking will be discussed in Section 3.2.3.

The only sample of intermediate composition in the range was "$TiNb_{14}O_{37}$." A few crystals of $Ti_2Nb_{10}O_{29}$ were identified by diffraction, but most of the *h*0*l* patterns from crystals in this sample were similar to that shown in Fig. 5c. The pattern possesses similarities to both $TiNb_{24}O_{62}$ (Fig. 2b) and monoclinic $Ti_2Nb_{10}O_{29}$ (Fig. 5a), but there is a pronounced streaking in the direction parallel to c^*.

3.2.2 *Electron Microscopy.* Lattice images of suitably tilted thin crystals of both forms of $Ti_2Nb_{10}O_{29}$ are shown in Fig. 6. When the 00*l* reflections alone were used (Fig. 6a,c), both forms gave identical images, with fringe spacings of 14.2 Å. However, faulting was revealed by tilting the crystals to include other reflections (Fig. 6b,d). In the monoclinic phase, the fringe spacing of 14.2 Å was retained except in the faulted regions, where the spacing was 28.5 Å. In the orthorhombic phase, the reverse situation applied.

A lattice image of $TiNb_{24}O_{62}$ using *h*00 reflections is shown in Fig. 3e. When the 00*l* reflections were used, a double set of fringes was observed. (Fig. 7a). The spacings were alternately 12 ± 1 and 9 ± 1 Å, and varied somewhat with the focussing conditions; however, the periodicity of the fringe pattern, 21 Å, was constant.

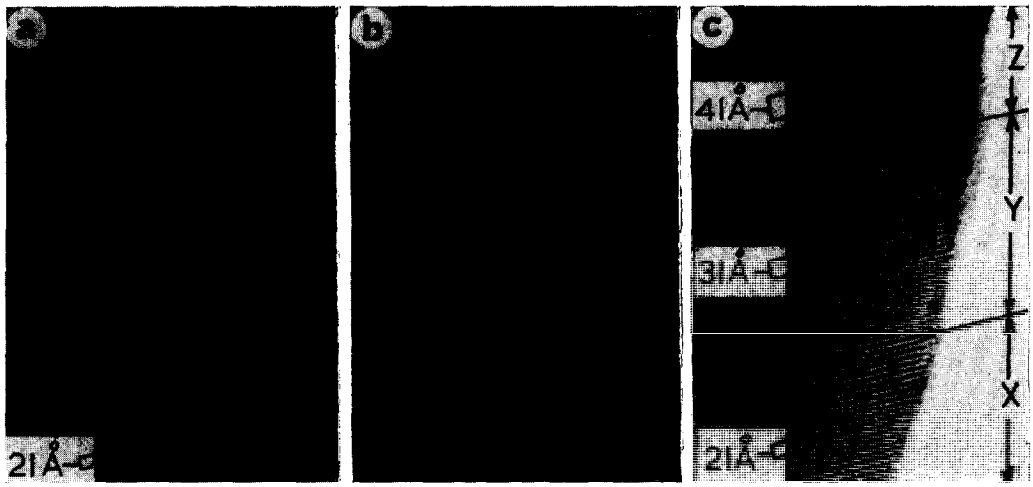

FIG. 7. Lattice images (Magnification 750,000×) from (a) $TiNb_{24}O_{62}$, using 00*l* reflections; (b) and (c) Two crystals in a sample of "$TiNb_{14}O_{37}$" showing random (b) and ordered (c) sequences of fringes. The Regions X, Y, and Z in (c) correspond to domains with compositions $TiNb_{24}O_{62}$, $Ti_3Nb_{34}O_{91}$ and $Ti_5Nb_{44}O_{120}$, respectively.

Crystals from the sample of "$TiNb_{14}O_{37}$," when viewed in the corresponding orientation, gave a variety of lattice images in which the wide and narrow fringes found in $TiNb_{24}O_{62}$ were distributed much less regularly. Figures 7b and c illustrate two typical cases. In addition to the simple sequence of fringes found in $TiNb_{24}O_{62}$ (e.g. Fig. 7a, X in Fig. 7c) several more complex ordered arrangements were observed. For example, the Region Y in Fig. 7c is ordered with a periodicity of 31 Å, and the Region Z has a repeat distance of 41 Å.

3.2.3 *Disorder in* $Ti_2Nb_{10}O_{29}$. The defects in $Ti_2Nb_{10}O_{29}$ (Fig. 6) are due to the presence of microdomains of one polymorph in the other. A model of the boundary between the orthorhombic and monoclinic forms is shown in Fig. 8. When viewed down the *a* axis, both structures appear the same and therefore the lattice images using 00*l* reflections (Fig. 6a,c) are identical. At other orientations, however, the two phases can be distinguished. In Fig. 6b,d, the fringes spaced 14.2 Å apart occur in regions of the monoclinic polymorph ($c\sin\beta = 14.25$ Å); those with a spacing of 28.5 Å correspond to regions of the orthorhombic phase ($c = 28.5$ Å).

3.2.4 *Intergrowth in* $TiNb_{24}O_{62}$ *and* "$TiNb_{14}O_{37}$." The double set of fringes in $TiNb_{24}O_{62}$ (Fig. 7a) and the more complex sequences in "$TiNb_{14}O_{37}$" (Fig. 7b,c) indicate that the intergrowth of two different structural units is occurring in these samples. However, this intergrowth differs from that found in the region between H–Nb_2O_5 and $TiNb_{24}O_{62}$ in the following ways:

(i) The intergrowing rows run parallel to *a* in $TiNb_{24}O_{62}$, whereas the C and D Rows described previously were parallel to *c* (Fig. 4a);

(ii) A comparison of microdensitometer records from micrographs of crystals of $TiNb_{52}O_{132}$ and "$TiNb_{14}O_{37}$" (Fig. 9) shows that in the former compound (and also in the intergrowth phase $W_4Nb_{26}O_{77}$ (*15*)) the *peak heights* vary, but in "$TiNb_{14}O_{37}$," the *depths of the valleys* vary. This

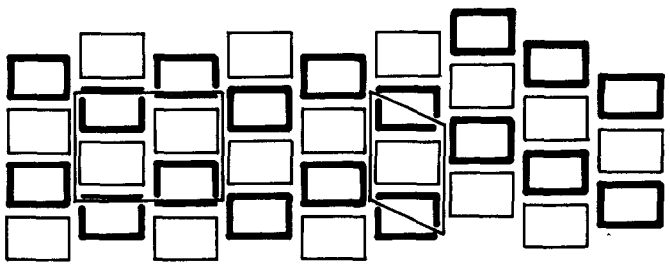

FIG. 8. Model of a boundary between the orthorhombic (left) and monoclinic (right) forms of $Ti_2Nb_{10}O_{29}$. The unit cell of each phase is outlined.

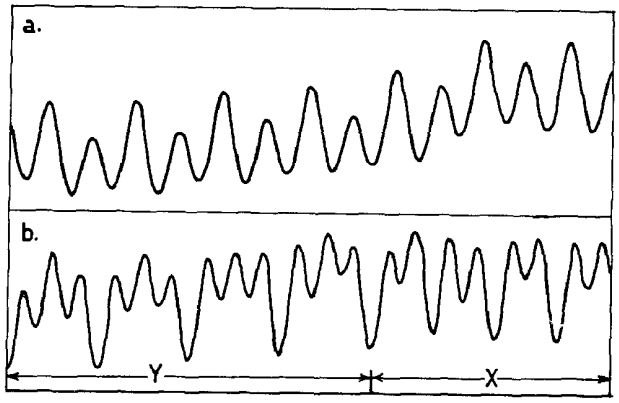

FIG. 9. Microdensitometer records taken across fringe sequences in lattice images of: (a) $TiNb_{52}O_{132}$—the valleys are alternately 15 Å and 17 Å apart. (b) "$TiNb_{14}O_{37}$"— corresponding to part of the Regions X and Y in Fig. 7(c).

produces an apparent variation in the width of white fringes in micrographs of $TiNb_{52}O_{132}$ (Fig. 3c) and of black fringes in "$TiNb_{14}O_{37}$" (Fig. 7b). An inspection of the structure of $TiNb_{24}O_{62}$ (Figs. 10c,1d) shows that in any plane of metal atoms perpendicular to *b*, there are rows of tetrahedral atoms separating blocks (E) and rows of junctions between blocks sharing octahedral edges (F), alternating regularly and running parallel to *a*. The structure can be considered as an intergrowth of two simpler structures, one in which all the blocks at any one level are separated by tetrahedral atoms (Fig. 10a) and the other in which there are no tetrahedral atoms, and all the blocks are joined by sharing edges (Fig. 10b). The former has the composition $M_{13}O_{33}$, and the compound $WNb_{12}O_{33}$ is known to have this structure (*1*). The latter is $M_{12}O_{29}$, exemplified by monoclinic $Ti_2Nb_{10}O_{29}$. These two

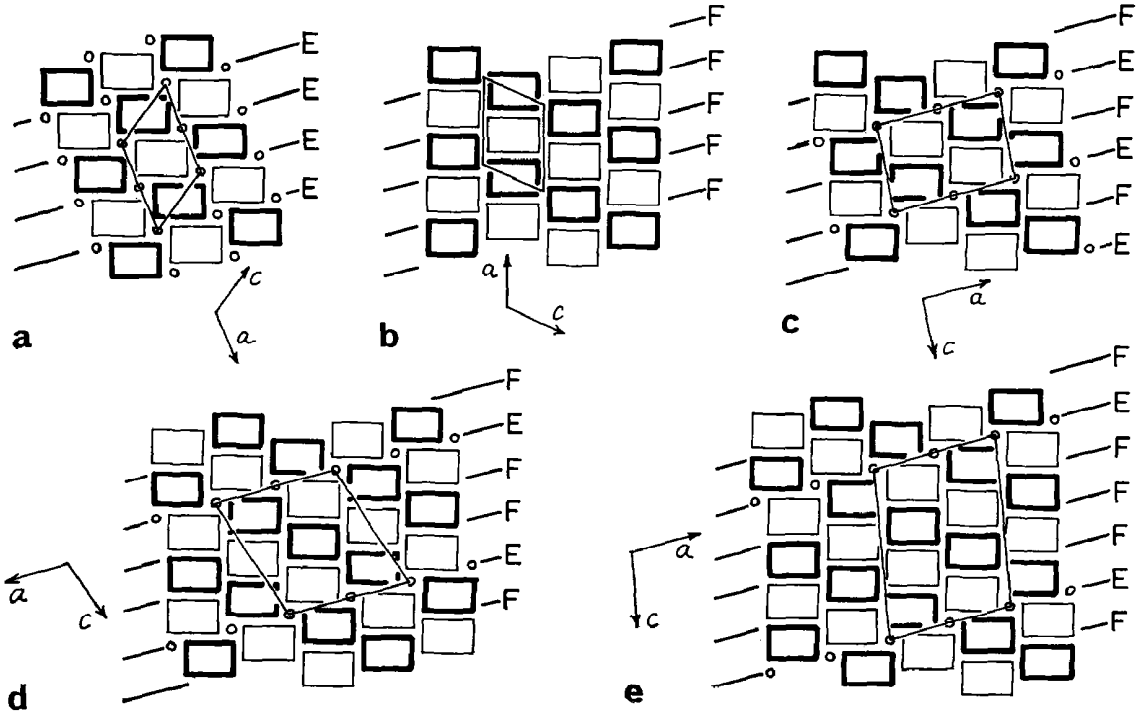

FIG. 10. Idealized models of: (a) the $M_{13}O_{33}$ structure; (b) the $M_{12}O_{29}$ structure; (c) $TiNb_{24}O_{62}$; (d) $Ti_3Nb_{34}O_{91}$; (e) $Ti_5Nb_{44}O_{120}$. The representation is similar to that used in Fig. 4. The parallel lines on either side of each structure mark the positions of shear planes of two types; E—in which the 4 × 3 blocks are separated by tetrahedral atoms (circles), and F—in which the blocks are joined by sharing octahedral edges.

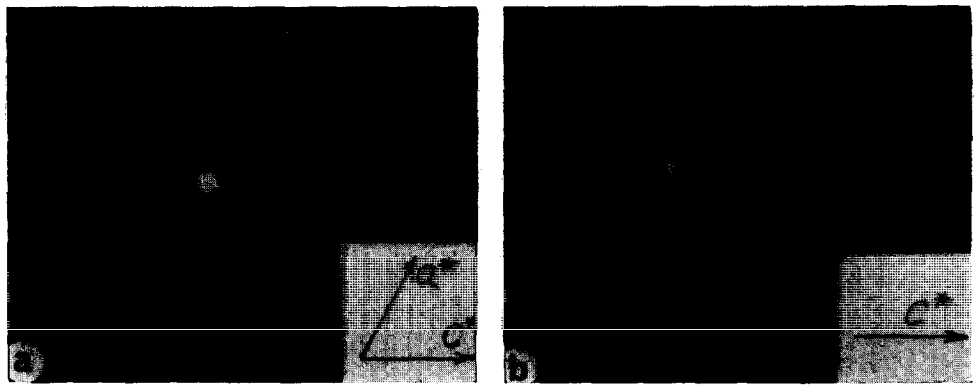

FIG. 11. Electron diffraction patterns (*h0l* sections) from (a) $TiNb_2O_7$; (b) a sample of $5TiO_2 \cdot 8Nb_2O_5$, after melting and annealing at 1300C.

compositions may be considered as the end-members of a series of possible intergrowths, containing various ordered sequences of rows of E and F type. Fig. 10c–e shows three different sequences, giving the compositions

$TiNb_{24}O_{62}$ (—E—F—E—F—E—),

$Ti_3Nb_{34}O_{91}$ (—E—F—F—E—F—F—E—), and

$Ti_5Nb_{44}O_{120}$

(—E—F—F—F—E—F—F—F—E—).

The braces identify the repeating unit in each case. These correspond to the observed sequences in Fig. 7c, in the Regions X, Y, and Z, respectively. The lines drawn on the models in Fig. 10, running parallel to *a* in $TiNb_{24}O_{62}$, represent the centers of black fringes in the micrographs in Fig. 7. The calculated distance between these lines is 11.0 Å across E-type rows, and 9.8 Å across F-type rows, giving periodicities of 20.8 Å for $TiNb_{24}O_{62}$, 30.6 Å for $Ti_3Nb_{34}O_{91}$, and 40.4 Å for $Ti_5Nb_{44}O_{120}$. These estimates agree well with the repeat distances in the Regions X, Y, and Z in Fig. 7c (21, 31 and 41 Å, respectively). The calculated unit cell dimensions of these three intergrowths are given in Table I. This interpretation is consistent with the previous discussion of intergrowth between H–Nb_2O_5 and $TiNb_{24}O_{62}$ (§3.1) in that in both cases, the peaks in the microdensitometer records (Fig. 9) (or the centers of white fringes in the micrographs) are correlated with the centers of blocks of octahedra, and the valleys (or centers of black fringes) correspond to the shear planes, where the density is higher than average. In the former case (Fig. 4), and also in the intergrowth phase $W_4Nb_{26}O_{77}$ (*15*), all the shear planes have the same structure, and the valleys in Fig. 9a are therefore of constant depth; the differences in peak height apparently reflect the differences in the width of the blocks or the distance between shear planes. However, in the $M_{13}O_{33}$–$M_{12}O_{29}$ intergrowths, the shear planes running parallel to the E and F Rows (Fig. 10) are of two kinds. In the E Rows, the planes contain tetrahedral atoms, which separate individual blocks of octahedra. In the F Rows, they contain junctions where the blocks are joined by sharing edges. Apparently it is this difference which produces pronounced changes in the depths of the valleys in the microdensitometer records (Fig. 9b).

3.3 The Region $Ti_2Nb_{10}O_{29}$–$TiNb_2O_7$

3.3.1 *Electron Diffraction.* The *h0l* patterns from crystals of $TiNb_2O_7$ (Fig. 11a) contained no sign of streaking which would indicate the presence of disorder. There is no evidence for polymorphism in this case, although an alternative structure, analogous to that of orthorhombic $Ti_2Nb_{10}O_{29}$ but built from 3 × 3 blocks, appears entirely reasonable.

Several samples with the composition $5TiO_2 \cdot 8Nb_2O_5$, close to a eutectic in the phase diagram (*6*), were also examined. Specimens which had been heated at temperatures below the solidus (e.g. 1400C for 16 hr), proved to be mixtures of $TiNb_2O_7$ and $Ti_2Nb_{10}O_{29}$, the latter giving streaked diffraction patterns indicative of disordered intergrowth of its two polymorphs (§3.2.3). Heavily streaked patterns (Fig. 11b) were obtained from a sample which had been melted and then annealed for several hours at 1300C. The streaks lay in the c^* direction and appeared in all the reciprocal lattice rows including 00*l*. The most significant difference between these patterns and those from disordered

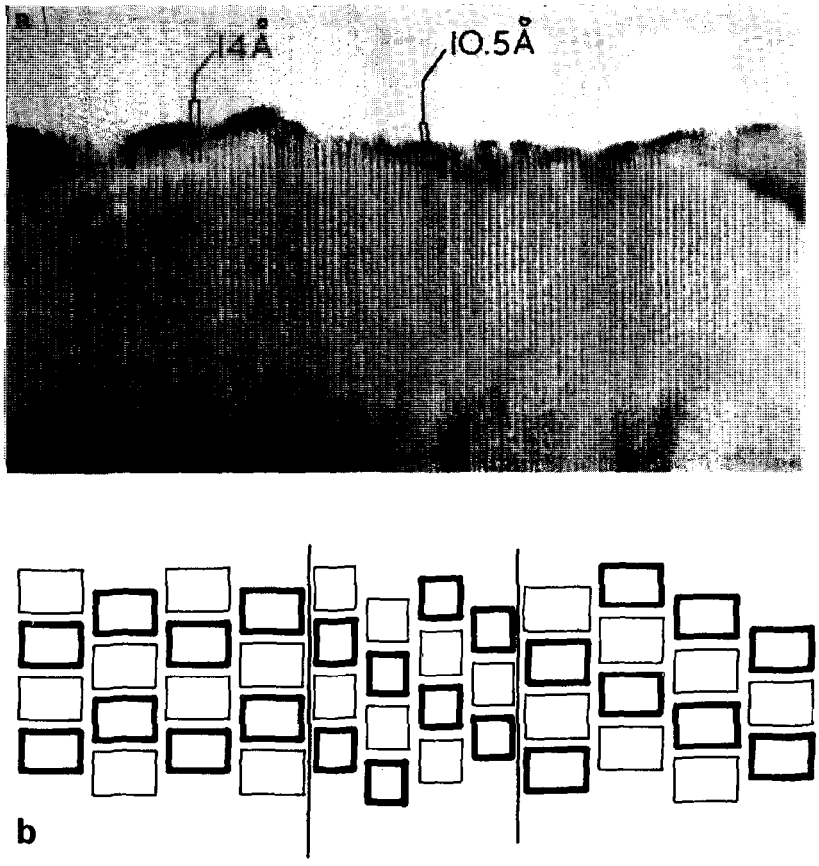

FIG. 12. (a) Lattice image of a fragment from a melted sample of $5TiO_2 \cdot 8Nb_2O_5$. Magnification: 750,000×. (b) Model showing possible structures for coherent boundaries between orthorhombic $Ti_2Nb_{10}O_{29}$ (left), $TiNb_2O_7$ (center) and monoclinic $Ti_2Nb_{10}O_{29}$ (right).

$Ti_2Nb_{10}O_{29}$ (Fig. 5a) was that in the latter case, the 00*l* reflections were *not* streaked.

3.3.2 *Electron Microscopy.* Crystal fragments from the melted sample of $5TiO_2 \cdot 8Nb_2O_5$ were examined in transmission using the 00*l* reflections. In this orientation, lattice images (Fig. 12a) consisted of parallel arrays of fringes with spacings of 14 Å and 10.5 Å. Periodicities of 28 Å were also observed when additional reflections were included. The sequence of the fringes and the proportion of each spacing varied considerably, even within a single fragment.

3.3.3 *The structure of the Eutectic* $5TiO_2 \cdot 8Nb_2O_5$. The electron optical observations of this material confirm the conclusions drawn by Wadsley (*14*) from his X-ray study. The structure of the material which had been melted may be described as a disordered intergrowth of $TiNb_2O_7$ (3 × 3 blocks) and the two polymorphs of $Ti_2Nb_{10}O_{29}$ (4 × 3 blocks). The fringe spacings of 14 Å and 10.5 Å in lattice images (Fig. 12a) correspond to blocks 4 octahedra and 3 octahedra wide, respectively; the expected spacings ($=c\sin\beta$) being 14.2 and 10.3 Å.

Microdomains of the orthorhombic form of $Ti_2Nb_{10}O_{29}$ are revealed by the presence of 28 Å fringes in lattice images of suitable oriented crystals. This effect has been discussed in Section 3.2.3. The coherent boundaries between $TiNb_2O_7$ and $Ti_2Nb_{10}O_{29}$ probably have structures similar to those illustrated by the model in Fig. 12b.

3.4 The Region $TiNb_2O_7$–TiO_2

A sample of composition $8TiO_2 \cdot 2Nb_2O_5$ was a mixture of $TiNb_2O_7$ and TiO_2. Because the structures of these two phases are quite different, it is very unlikely that intergrowth would be possible. For this reason, this region of the phase diagram was not

studied in detail. TiO_2 is reported to accept up to 17% Nb_2O_5 into solid solution (*6*), but the structure in this range of composition was not investigated further.

4. Discussion

4.1 Comparison with Previous Work

The electron optical observations which have been described confirm most of the earlier X-ray work in this system. The electron diffraction patterns of the pure phases $TiNb_{24}O_{62}$, $Ti_2Nb_{10}O_{29}$ (both forms) and $TiNb_2O_7$ are completely consistent with the previously published crystallographic constants of these materials (Table I). There is no evidence in these patterns for the presence of superlattices or diffuse reflections which might indicate that there is some ordering of the Nb and Ti atoms. Hence the earlier assumption that these elements occupy the metal atom positions randomly is supported.

The question of the structure and composition of $TiNb_{52}O_{132}$ has been examined in some detail, and all the evidence is consistent with the idealized structure proposed in this paper (Fig. 4h). There is no indication that the composition of this phase differs from that determined from the contents of the idealized unit cell. However, because it seems almost impossible to prepare pure, homogeneous samples of any of these intergrowth phases, their compositions have not yet been confirmed by direct analysis. The fact that Gruehn's sample of $(Ti,Nb)O_{2.483}$ contains significant amounts of $TiNb_{24}O_{62}$ and the more complex ordered intergrowth $TiNb_{38}O_{97}$ (Fig. 3d) in the form of microdomains coexisting with $TiNb_{52}O_{132}$ may explain the discrepancy between his chemically determined composition and the value deduced from the proposed structure. It is clear that the techniques used in the present investigation are considerably more sensitive than the commonly used X-ray powder diffraction methods. There are several reasons for this:

(a) Electron diffraction patterns from very small fragments of single crystals contain very much more information than powder diffraction patterns. Even if single crystal X-ray data are available, they are frequently less complete than electron diffraction data, because of the long exposure times required to record very weak diffracted intensities from small crystals. Disorder, causing diffuse streaking in diffraction patterns, is easily recorded with electrons, but would frequently pass unnoticed with X-rays.

(b) The observation of lattice images permits the resolution of the structure at the unit cell level, or better. The contrast in these images of thin crystals which behave as phase gratings (*18*) is not dependent upon the presence of periodicity in the crystals; hence nonperiodic faults are clearly revealed. Microdomains of impurity phases in a matrix are readily identified, but their presence would cause at most a slight broadening of X-ray diffraction lines. Because of the small size of these domains, and the complexity and similarity of the diffraction patterns of closely related series of compounds such as the intergrowths described here, the usual criterion for the presence of a single phase, i.e. the absence of foreign reflections in X-ray powder diffraction data, is not particularly sensitive. This is undoubtedly the reason why $TiNb_{24}O_{62}$ was overlooked in the original phase analysis—the phase diagram reported by Roth and Coughanour (*6*) contained a region of solid solution in Nb_2O_5 up to about 12 mole percent TiO_2, followed by a two phase region (Nb_2O_5 solid solution plus $Ti_2Nb_{10}O_{29}$).

4.2 Non-stoichiometry and Intergrowth

The "solid solution" of TiO_2 in Nb_2O_5, which has a variable composition, has proved to be a series of intergrowth structures. These structures contain the elements of several simpler, but closely related parent structures, in the form of thin slabs. Any composition within the range between the two parent structures may in principle, be obtained by suitably combining the appropriate proportions of these slabs, either randomly or in an ordered sequence. The slabs fit together at shear planes with no more difficulty than they do in the parent structures, and there is no need to postulate the existence of vacant sites or interstitial atoms of any kind so as to explain the observed ranges of composition or non-stoichiometry. The simplest ordered intergrowths, containing equal numbers of slabs of each parent are $TiNb_{24}O_{62}$ (Figs. 3e, 7a) and $TiNb_{52}O_{132}$ (Fig. 3c). These phases, particularly the former, were relatively easy to prepare and large domains of unfaulted material occurred frequently. The more complex ordered sequences such as $TiNb_{38}O_{97}$ (Fig. 3d,e) $Ti_3Nb_{34}O_{91}$ and $Ti_5Nb_{44}O_{120}$ (Fig. 7c) were found only as small domains, and were often surrounded by regions of random intergrowth. The driving force for the ordering process is probably very small, and it is likely that long annealing times under carefully controlled conditions are required to produce homogeneous samples of these and possibly other complex intergrowths.

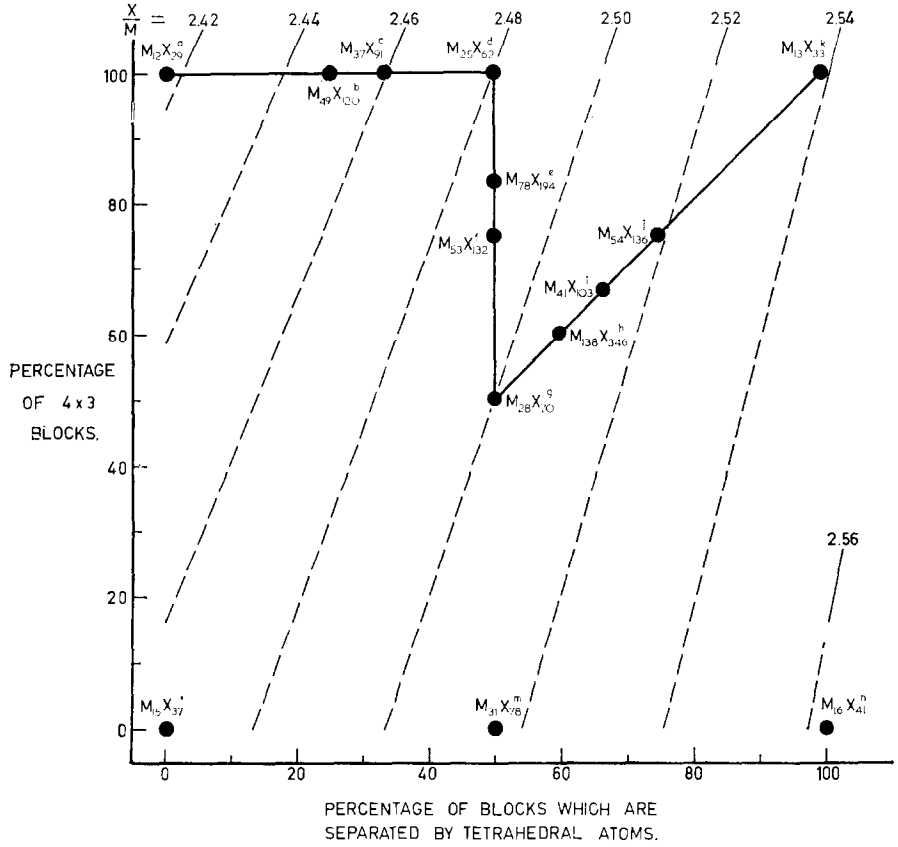

FIG. 13. Known structures containing 4 × 3 and 5 × 3 blocks of octahedra. The dashed lines are lines of constant non-metal (X) to metal (M) ratio. The solid lines indicate regions where intergrowth has been observed. Compositions of known phases are represented by circles. The superscripts on each of these compositions identify these phases as follows: (a) $Ti_2Nb_{10}O_{29}$ (*8*); (b) $Ti_5Nb_{44}O_{120}$ (this work); (c) $Ti_3Nb_{34}O_{91}$ (this work); (d) $TiNb_{24}O_{62}$ (*10*); (e) $TiNb_{38}O_{97}$ (this work); (f) $TiNb_{52}O_{132}$ (*11*, this work); (g) H–Nb_2O_5 (*12*); (h) $WNb_{68}O_{173}$ (*5*); (i) $WNb_{40}O_{103}$ (*5*); (j) $WNb_{26}O_{68}$ (*5*); (k) $WNb_{12}O_{33}$ (*1*); (l) $MgNb_{14}O_{35}F_2$ (*13*); (m) $Nb_{31}O_{77}F$ (*19*); (n) $MoNb_{15}O_{40}F$ (*20*).

4.3 Other Possible Intergrowths

The parent structures containing 4 × 3 and 5 × 3 blocks of octahedra, and the known ordered intergrowths of these parents in the H–Nb_2O_5 family are shown in Fig. 13. Iso-composition lines are also drawn on this diagram and it is clear that, for a particular composition M_aX_b, there are a number of possible structures (apart from those made from blocks with sizes other than 4 × 3 and 5 × 3). For example the M_2X_5 composition is produced by intergrowing either $M_{12}X_{29}$·2($M_{13}X_{33}$), $M_{15}X_{37}$·$M_{13}X_{33}$ (as in H–Nb_2O_5), or 2($M_{15}X_{37}$)·$M_{16}X_{41}$, and there are other more complex possibilities. It seems quite likely that many additional structures of this kind could be prepared by choosing appropriate conditions and materials. The reason for the occurrence of one particular series of intergrowths when there are several obvious alternatives is not at all

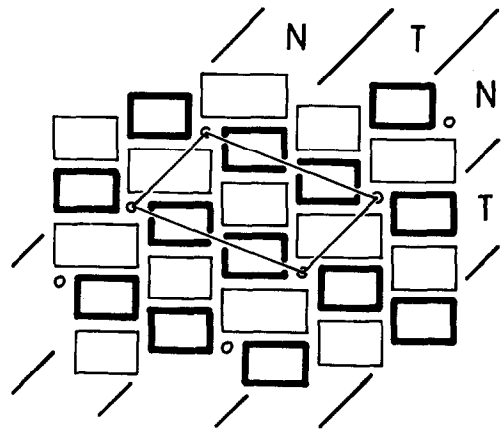

FIG. 14. Model of $Ti_2Nb_{24}O_{64}$, a theoretically-possible intergrowth of $Ti_2Nb_{10}O_{29}$ (labeled T) and H–Nb_2O_5 (labeled N).

clear. In the region $Ti_2Nb_{10}O_{29}$–Nb_2O_5, for example, a series on the direct path between $M_{12}X_{29}$ and $M_{28}O_{70}$ appears a very reasonable possibility. The structure of an ordered intergrowth of Nb_2O_5 and $Ti_2Nb_{10}O_{29}$ having the composition $Ti_2Nb_{24}O_{64}$ is shown in Fig. 14. An alternative route would be via $M_{15}X_{37}$; the compound $TiNb_{14}O_{37}$, having this stoichiometry was proposed by Wadsley (*8*), but has not been found in the TiO_2–Nb_2O_5 system.

5. Acknowledgement

I am indebted to Dr. R. Gruehn for providing samples of $(Ti,Nb)O_{2.483}$ and $NbO_{2.483}$, and to Dr. J. V. Sanders for helpful discussions. I wish to record that this work was suggested by Dr. A. D. Wadsley, who, with his penetrating insight into solid state problems, coupled with tremendous enthusiasm, was a constant source of advice and encouragement. He personally criticized this manuscript shortly before his death.

References

1. R. S. Roth and A. D. Wadsley, *Acta Cryst.* **19**, 26, 32, 38 (1965).
2. S. Andersson, W. G. Mumme, and A. D. Wadsley, *Acta Cryst.* **21**, 802 (1965).
3. H. J. Goldschmidt, *Metallurgia* **62**, 373 (1960).
4. H. J. Goldschmidt, "Interstitial Alloys," p. 420. Butterworth, London, (1960).
5. J. G. Allpress and A. D. Wadsley, *J. Solid State Chem.* **1**, 28 (1969).
6. R. S. Roth and L. W. Coughanour, *J. Res. Nat. Bur. Stand.* **55**, 209 (1955).
7. A. D. Wadsley, *Acta Cryst.* **14**, 660 (1961).
8. A. D. Wadsley, *Acta Cryst.* **14**, 664 (1961).
9. R. Gruehn and H. Schäfer, *Naturwiss.* **50**, 642 (1963).
10. R. S. Roth and A. D. Wadsley, *Acta Cryst.* **18**, 724 (1965).
11. R. Gruehn and R. Norin, *Z. Anorg. Allgem. Chem.* **355**, 176 (1967).
12. B. M. Gatehouse and A. D. Wadsley, *Acta Cryst.* **17**, 1545 (1964).
13. M. Lundberg (to be published).
14. A. D. Wadsley, *in* "Non-Stoichiometric Compounds" (L. Mandelcorn, Ed.) p. 161. Academic Press, New York (1964).
15. J. G. Allpress, J. V. Sanders, and A. D. Wadsley, *Acta Cryst.* (in press).
16. G. W. C. Milner, G. A. Bartlett, and A. A. Smales, *Analyst*, **80**, 380 (1955).
17. S. Andersson and A. D. Wadsley, *Nature* **211**, 581 (1966).
18. J. M. Cowley and A. F. Moodie, *Proc. Phys. Soc.* **76**, 382 (1960).
19. A. Astrom, *Acta Chem. Scand.* **20**, 969 (1966).
20. J. Galy and S. Andersson, *Acta Cryst.* **B24**, 1027 (1968).